UCRL- 95895
PREPRINT

BOUNDARY-PROJECTION ACCELERATION: A NEW APPROACH TO SYNTHETIC ACCELERATION OF TRANSPORT CALCULATIONS

MARVIN L. ADAMS
WILLIAM R. MARTIN

THIS PAPER PREPARED FOR SUBMITTAL TO
NUCLEAR SCIENCE & ENGINEERING
PARIS, FRANCE
MAY 1987

JANUARY 1987

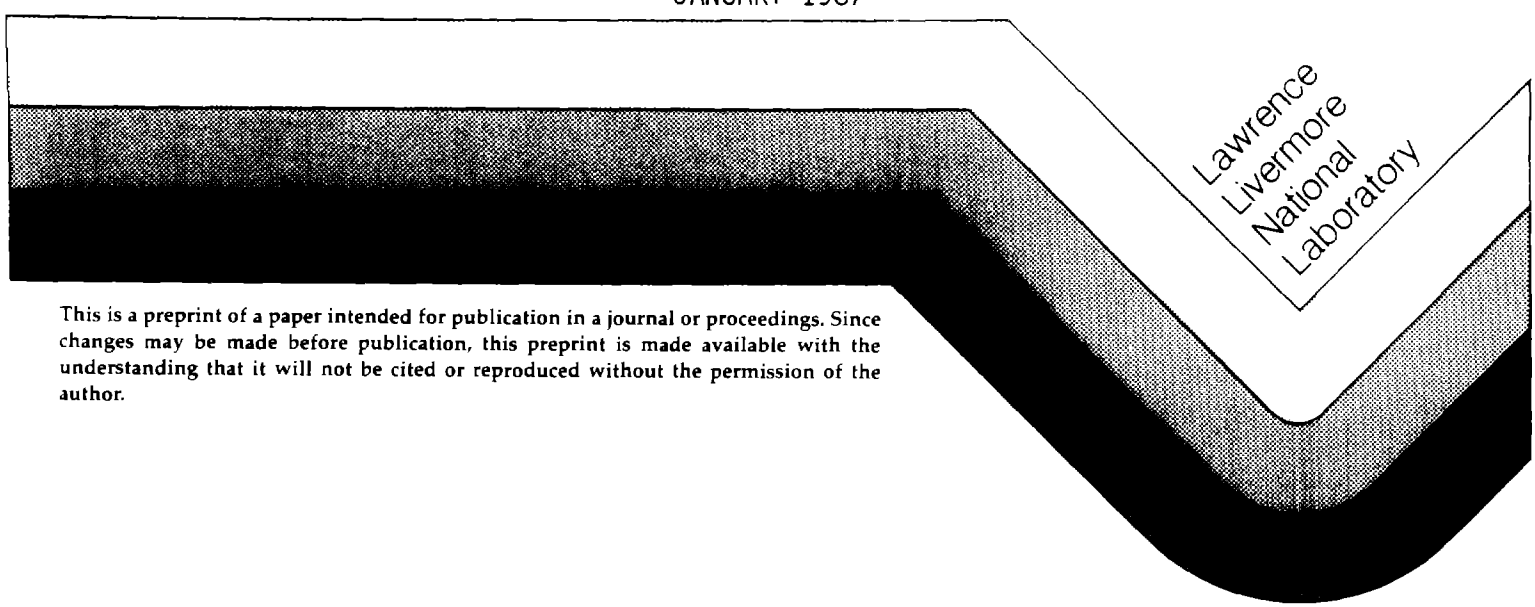

BOUNDARY-PROJECTION ACCELERATION: A NEW APPROACH TO SYNTHETIC ACCELERATION OF TRANSPORT CALCULATIONS

Marvin L. Adams
Lawrence Livermore National Laboratory
P. O. Box 808, L-419
Livermore, CA 94550
(415) 423-9846

William R. Martin
Department of Nuclear Engineering
The University of Michigan
Ann Arbor, MI 48109
(313) 764-5534

ABSTRACT

We present a new class of synthetic acceleration methods which can be applied to transport calculations regardless of geometry, discretization scheme, or mesh shape. Unlike other synthetic acceleration methods which base their acceleration on P1 equations, these methods use acceleration equations obtained by *projecting* the transport solution onto a coarse angular mesh *only on cell boundaries*. We demonstrate, via Fourier analysis of a simple model problem as well as numerical calculations of various problems, that the simplest of these methods are unconditionally stable with spectral radius $\leq c/3$ (c being the scattering ratio), for several different discretization schemes in slab geometry.

I. INTRODUCTION

The numerical solution procedure for realistic neutral-particle transport problems is necessarily iterative; most methods in use today iterate on the scattering source[1-4]. It is well understood that an unaccelerated scattering-source iteration can converge arbitrarily slowly: for model (infinite medium, constant cross-section, constant mesh spacing, isotropic scattering) problems the spectral radius is c, the scattering ratio, which can be arbitrarily close to unity[5]. Hence, many techniques for accelerating this iteration have been proposed[5-21]. Each of these methods involves, within each full iteration, a fixed-source transport calculation followed by an "acceleration" calculation designed to improve the transport result. The methods which have been most successful make use of a "low-order" approximation to the transport equation (such as the diffusion equation) in their acceleration calculations; these are called *synthetic* acceleration methods[5,8,9-21].

The idea behind synthetic acceleration can be explained as follows. Given an equation of the form

$$[A - B]\, f = s, \tag{1}$$

where it is difficult to invert [A – B] but relatively easy to invert A, we might try the iterative scheme

$$f^{l+1} = M f^{l} + A^{-1}s, \tag{2}$$

where $M = A^{-1}B$ and l is the iteration index. The eigenvalues of M determine the convergence properties of this iteration. In particular, if the magnitude of the largest eigenvalue (the "spectral radius") is less than unity the iteration will converge regardless of the starting guess; otherwise, it will not.

If we denote the converged solution as f (no superscript), then it is easy to show that

$$[A - B](f - f^{l+1}) = B(f^{l+1} - f^{l}). \tag{3}$$

That is, the converged solution f is obtainable at any time (if one is willing to invert [A – B]) given only the knowledge of two successive iterates. Of course, we are not interested in inverting [A–B], but suppose there exists a "low-order" approximation, L, to the "high-order" operator [A – B], with L easily invertible. Then eqns. (2) and (3) suggest the following iteration scheme:

$$f^{l+1/2} = M f^{l} + A^{-1}s, \tag{4a}$$
$$L(f^{l+1} - f^{l+1/2}) = B(f^{l+1/2} - f^{l}). \tag{4b}$$

This is synthetic acceleration[6,8]. The logic is simple: if L is "close" to [A – B], then f^{l+1} should be "close" to the converged solution f.

Synthetic acceleration of transport iterations was first proposed by Kopp[6] in 1963, who used the diffusion equation as his low-order approximation to the transport equation. In this case eqns. (4) become

$$[\underline{\Omega}\bullet\underline{\nabla} + \sigma_t]\,\psi^{l+1/2} = \sigma_s \phi_0^{l} + q, \tag{5a}$$

$$[-\underline{\nabla}\bullet D\underline{\nabla} + \sigma_a](\phi_0^{l+1} - \phi_0^{l+1/2}) = \sigma_s(\phi_0^{l+1/2} - \phi_0^{l}) \tag{5b}$$

Kopp's work, which was limited to the continuous slab-geometry equations, was extended and applied to the discretized S_N equations by Gelbard and Hageman[7], who found that the synthetic method worked well in XY geometry for small meshes but reported no numerical results for large meshes. Reed[8] later showed that, given the diamond-differenced transport equation and a centrally-differenced diffusion equation, the synthetic iteration could diverge for meshes larger than about 1.2 mean-free paths (mfp's).

Alcouffe recognized in the mid-1970s that the reason for this instability was an inconsistency in the differencing of the transport and diffusion equations; through careful "consistent" differencing of the diffusion equation he was able to construct a diffusion-synthetic acceleration (DSA) technique for

the diamond-differenced transport equation that was stable for all mesh sizes, with spectral radius less than 0.23c for a simple model problem[5,10]. Alcouffe actually created three different DSA schemes, two of which are always nonlinear, the third being nonlinear in general but linear for some problems (such as the model problem)[10]. The nonlinearities arise because some parameters in Alcouffe's acceleration equations require division by fluxes from the most recent transport calculation. This forces the use of a negative-flux fixup, for negative or zero fluxes could be disastrous; however, if too many fixups are used the iteration diverges -- the fixups effectively alter the transport differencing scheme, making it inconsistent with the acceleration equations[15].

Conceptually, Alcouffe's method can be applied to any transport differencing scheme regardless of geometry or mesh shape. At this point, however, it has not been attempted on a non-orthogonal mesh[22]; further, an extension to the linear characteristic differencing scheme produced a method which was unstable for large meshes[22,23]. Thus, it is not yet clear whether the method is generally useful for non-diamond differencing and/or non-orthogonal meshes.

In the early 1980s, Larsen extended Alcouffe's reasoning and created a "four-step procedure" whereby one could derive, beginning with virtually any differencing of the transport equation, a consistently-differenced set of *linear* P1 acceleration equations which yielded spectral radii less than c/3 (for the model problem in slab geometry)[5,14,15]. Larsen's scheme can be applied to virtually any transport differencing scheme, apparently without regard to geometry or mesh shape; in these regards it represents a significant advance over the earlier nonlinear methods. However, the P1 acceleration equations are in general algebraically complicated -- it has yet to be shown that they can be solved efficiently enough to warrant their use[5] -- whereas the diffusion equation used by Alcouffe's nonlinear DSA method is amenable to solution by a very efficient multigrid scheme.

Recently Khalil presented a nodal DSA method whereby nodally-differenced transport iterations can be accelerated by nodally-differenced diffusion equations[17]. Khalil's acceleration equations appear to have the same form as Larsen's, but his method differs from that of Larsen in the way that those equations are derived[24]. While it appears that Khalil's method is rapidly convergent, his acceleration equations may be just as difficult to solve efficiently, in general, as are Larsen's.

In summary, no acceleration technique developed to date has been shown to possess all of the following desired properties:

1) Unconditional stability and rapid convergence (i.e., spectral radius significantly less than unity for all mesh sizes),
2) Generality with respect to geometry,
3) Generality with respect to discretization scheme,
4) Generality with respect to mesh shape,
5) Easily-solved low-order equation,
6) Accelerated solution equal to unaccelerated solution.

Alcouffe's nonlinear DSA apparently possesses properties 2, 3, 4, 5, and 6; property 1 has been shown only for diamond differencing on an orthogonal mesh when fixups do not overwhelm the method. Larsen's 4-step DSA appears to have all properties except 5, which is of course crucial.

Khalil's nodal DSA appears to possess the same properties as Larsen's method, although 2, 3, and 4 are not certain[24]. (We note that further research into these acceleration methods may eliminate some of the drawbacks listed here.) Property 6, which all true acceleration methods possess, has been included to distinguish the methods discussed in this paper from a related class of rapidly-convergent schemes (not true acceleration techniques) which have been called "projected discrete-ordinates" methods[25].

As a step toward fulfilling all six of the above criteria, we present here a class of synthetic acceleration methods for transport calculations which differs from earlier methods in the choice of a low-order operator. Instead of using P1 or diffusion equations, we derive (beginning with the discretized transport equation) acceleration equations by *projecting* the transport solution onto a coarse angular mesh *only on cell boundaries*. We refer to methods generated in this manner as "boundary-projection acceleration" (BPA) methods. We note that Lawrence, working independently, has developed a BPA method which he calls "interface-current synthetic acceleration" (ICSA)[19]; he has obtained promising numerical results with a variety of transport differencing schemes in slab geometry, and with various nodal transport schemes in XY and XYZ geometries.

We show here that BPA methods can be applied regardless of geometry, discretization, or mesh shape (properties 2, 3, and 4). We also show, via numerical results as well as Fourier analyses of the model problem, that in slab geometry the BPA methods are unconditionally stable and rapidly convergent (property 1), with the simplest method having a spectral radius $\leq c/3$. (This is true only if the *projection* is done properly.) We argue that similar results can be expected in other geometries, although the acceleration equations may be necessarily more complicated. The remaining question is the ease of solution of the acceleration equations (property 5); we show that the acceleration equations are easily put into a form convenient for iteration on interface quantities, but the question of how efficiently this iteration can be performed is left for further research.

In section II we give a general-geometry, general-discretization, general-mesh, 4-step derivation of a fairly general BPA method, borrowing the philosophy and terminology of Larsen's 4-step DSA procedure. (This derivation serves as our proof that the method possesses properties 2, 3, and 4.) In section III we present details of the slab-geometry implementation of the method, paying close attention to the crucial *projection* step. Section IV contains results from slab-geometry model-problem Fourier analyses of weighted-diamond, linear discontinuous, and linear moments discrete-ordinates transport schemes accelerated by a few simple BPA methods; numerical results verifying the analyses are also presented. We draw conclusions in section V, noting areas that need further study.

II. GENERAL DERIVATION

As mentioned above, the basic idea behind synthetic acceleration is the use of a "low-order" equation to accelerate the convergence of a "high-order" iteration. With DSA schemes, high-order means transport and low-order means P1 or diffusion. Equivalently, high-order means *fine-mesh in angle* and low-order means *coarse-mesh (linearly anisotropic) in angle*. With the BPA schemes

described here, high-order also means fine-mesh in angle and low-order also means coarse-mesh in angle, but the coarse angular mesh of the low-order equation is imposed *only on cell boundaries*. Furthermore, the coarse mesh is not restricted to the P1 space, but is left to the imagination.

We begin our derivation of the BPA method with the *discretized* within-group transport equation (assuming isotropic scattering, for simplicity) written in the following form:

$$\underline{\Phi}_{o,i}^{l+1/2} = T_v^i \underline{\Phi}_{o,i}^{l} + T_b^i \underline{\Psi}_{in,i}^{l+1/2} + \underline{S}_{v,i} \tag{6a}$$

$$\underline{\Psi}_{out,i}^{l+1/2} = R_v^i \underline{\Phi}_{o,i}^{l} + R_b^i \underline{\Psi}_{in,i}^{l+1/2} + \underline{S}_{b,i} \tag{6b}$$

where
- $\underline{\Phi}_{o,i}$ = vector of scalar flux unknowns in the interior of cell i,
- $\underline{\Psi}_{in(out),i}$ = vector of incoming (outgoing) angular fluxes on the boundary of cell i,
- $\underline{S}_{v,i}$ = contribution from the external, fission, and inscatter sources to the scalar flux in the interior of cell i,
- $\underline{S}_{b,i}$ = contribution from the external, fission, and inscatter sources to the outgoing angular flux on the boundary of cell i,
- R_v^i = matrix giving the first-flight contribution to the outgoing angular flux due to within-group scattering in cell i,
- R_b^i = matrix giving the first-flight contribution to the outgoing angular flux due to the incoming flux on the boundary of cell i,
- T_v^i = matrix giving the first-flight contribution to the scalar flux in cell i due to within-group scattering in cell i,
- T_b^i = matrix giving the first-flight contribution to the scalar flux in cell i due to the incoming flux on the boundary of cell i,

with l the iteration index. With the exception of nonlinear schemes such as the exponential method[26], almost any transport discretization in any geometry (regardless of mesh shape) can be written in this form -- it is simply a statement of linearity.

We proceed by defining a coarse mesh and creating *projection matrices* which take us back and forth between fine- and coarse-mesh function spaces:

- $P^i_{f\leftarrow c}$ = coarse-to-fine "projection" matrix for the incoming boundary of cell i; gives a fine-mesh representation of the coarse-mesh flux,
- $P^i_{c\leftarrow f}$ = fine-to-coarse projection matrix for the outgoing boundary of cell i; projects the fine-mesh flux onto the coarse mesh.

We define coarse-mesh boundary fluxes and an incoming "residual" as follows:

$$\underline{J}_{out,i}^{l+1/2} = \text{vector containing coarse-mesh outgoing flux unknowns, cell } i$$
$$= P^i_{c\leftarrow f}\ \underline{\Psi}_{out,i}^{l+1/2} \tag{7a}$$

$$\underline{\Psi}_{res,i}^{l+1/2} = \text{incoming flux "residual"}$$
$$= \underline{\Psi}_{in,i}^{l+1/2} - P^i_{f\leftarrow c}\,\underline{J}_{in,i}^{l+1/2} \tag{7b}$$

With these definitions, we are ready to proceed with a four-step BPA procedure which is much like Larsen's four-step DSA procedure.

Step 1 -- Project onto coarse mesh. We replace $\underline{\Psi}_{in,i}^{l+1/2}$ in eqns. (6a) and (6b) using the definition eqn. (7b), then operate on eqn. (6b) with $P^i_{c\leftarrow f}$, obtaining:

$$\underline{\Phi}_{oi}^{l+1/2} = T_v^i\,\underline{\Phi}_{oi}^{l} + T_b^i\,[P^i_{f\leftarrow c}\,\underline{J}_{in,i}^{l+1/2} + \underline{\Psi}_{res,i}^{l+1/2}] + \underline{S}_{v,i} \tag{8a}$$

$$\underline{J}_{out,i}^{l+1/2} = P^i_{c\leftarrow f}\,R_v^i\,\underline{\Phi}_{oi}^{l} + P^i_{c\leftarrow f}\,R_b^i\,[P^i_{f\leftarrow c}\,\underline{J}_{in,i}^{l+1/2} + \underline{\Psi}_{res,i}^{l+1/2}] + P^i_{c\leftarrow f}\,\underline{S}_{b,i} \tag{8b}$$

Step 2 -- Define acceleration equations. We change all iteration indices, except that of the incoming residual, to l+1:

$$\underline{\Phi}_{oi}^{l+1} = T_v^i\,\underline{\Phi}_{oi}^{l+1} + T_b^i\,[P^i_{f\leftarrow c}\,\underline{J}_{in,i}^{l+1} + \underline{\Psi}_{res,i}^{l+1/2}] + \underline{S}_{v,i} \tag{9a}$$

$$\underline{J}_{out,i}^{l+1} = P^i_{c\leftarrow f}\,R_v^i\,\underline{\Phi}_{oi}^{l+1} + P^i_{c\leftarrow f}\,R_b^i\,[P^i_{f\leftarrow c}\,\underline{J}_{in,i}^{l+1} + \underline{\Psi}_{res,i}^{l+1/2}] + P^i_{c\leftarrow f}\,\underline{S}_{b,i} \tag{9b}$$

Step 3 -- Subtract unaccelerated equations from accelerated equations:

$$\underline{f}_{oi}^{l+1} = T_v^i\,(\underline{\Phi}_{oi}^{l+1} - \underline{\Phi}_{oi}^{l}) + T_b^i\,P^i_{f\leftarrow c}\,\underline{b}_{in,i}^{l+1} \tag{10a}$$

$$\underline{b}_{out,i}^{l+1} = P^i_{c\leftarrow f}\,R_v^i\,(\underline{\Phi}_{oi}^{l+1} - \underline{\Phi}_{oi}^{l}) + P^i_{c\leftarrow f}\,R_b^i\,P^i_{f\leftarrow c}\,\underline{b}_{in,i}^{l+1} \tag{10b}$$

where
$$\underline{f}_{oi}^{l+1} \equiv \underline{\Phi}_{oi}^{l+1} - \underline{\Phi}_{oi}^{l+1/2}$$
$$\underline{b}_{in(out),i}^{l+1} \equiv \underline{J}_{in(out),i}^{l+1} - \underline{J}_{in(out),i}^{l+1/2}.$$

Step 4 -- Manipulate the acceleration equations (10) into a form convenient for solution. First we rewrite (10a) as follows:

$$\underline{f}_{oi}^{l+1} = [I - T_v^i]^{-1}\,(T_v^i\,\underline{\delta\Phi}_{oi}^{l+1/2} + T_b^i\,P^i_{f\leftarrow c}\,\underline{b}_{in,i}^{l+1}), \tag{11}$$

where we have defined $\underline{\delta\Phi}_{oi}^{l+1/2} \equiv \underline{\Phi}_{oi}^{l+1/2} - \underline{\Phi}_{oi}^{l}$ and noted that $\underline{\Phi}_{oi}^{l+1} - \underline{\Phi}_{oi}^{l} = \underline{f}_{oi}^{l+1} + \underline{\delta\Phi}_{oi}^{l+1/2}$. Next we insert eqn. (11) into eqn. (10b) to obtain:

$$\underline{b}_{out,i}^{l+1} = M_{b,i}\,\underline{b}_{in,i}^{l+1} + M_{v,i}\,\underline{\delta\phi}_{oi}^{l+1/2} \tag{12}$$

where
$$M_{b,i} = P^{i}_{c\leftarrow f} R_b^{i} P^{i}_{f\leftarrow c} + P^{i}_{c\leftarrow f} R_v^{i} [I - T_v^{i}]^{-1} T_b^{i} P^{i}_{f\leftarrow c}$$
$$M_{v,i} = P^{i}_{c\leftarrow f} R_v^{i} + P^{i}_{c\leftarrow f} R_v^{i} [I - T_v^{i}]^{-1} T_v^{i}$$

Equation (12) is amenable to solution via iteration on the interface quantities $\underline{b}_{in(out)}$; upon convergence of this iteration, equation (11) can be used to obtain the cell-interior quantities $\underline{f}_o$ which are then used to update the scalar fluxes for the next iteration.

Implicit in the above derivation is the assumption that the coarse-mesh function space at any point on a cell boundary can be separated into two distinct half-spaces. That is, the coarse-mesh unknowns are clearly divided at cell boundaries into an "incoming" set which depends only on incoming angular fluxes and an "outgoing" set which depends only on outgoing fluxes. This assumption precludes the use of the P1 function space, for example, because the P1 unknowns are *full-range* integrals of the angular flux. We stress that this assumption is not necessary for the implementation of the BPA method; it merely simplifies the derivation a bit. Curious readers may see the fully general derivation in the appendix.

We have thus far ignored the details of the crucial projection matrices as well as the economics of solving the acceleration equations (11) and (12). We have also ignored an even more fundamental question: will the BPA methods work? The question of projections will be addressed in the next section; the question of economics will be discussed briefly in Section V, but essentially left as an area for further research. The question of how well the BPA methods work is answered, for slab geometry, in Section IV.

III. IMPLEMENTATION IN SLAB GEOMETRY

The BPA equations, derived above for the general case, will be developed here in detail for the diamond-differenced discrete-ordinates transport equation with isotropic scattering in slab geometry, which is written:

$$\frac{\mu_m}{\Delta x_i}\left(\psi_{mi+1/2}^{l+1/2} - \psi_{mi-1/2}^{l+1/2}\right) + \sigma_i\,\psi_{mi}^{l+1/2} = \sigma_{si}\,\phi_{oi}^{l} + q_{mi} \tag{13a}$$

$$\psi_{mi}^{l+1/2} = \frac{1}{2}\left(\psi_{mi+1/2}^{l+1/2} + \psi_{mi-1/2}^{l+1/2}\right) \tag{13b}$$

$$\phi_{oi}^{l+1/2} = \sum_{m=1}^{M} w_m\,\psi_{mi}^{l+1/2} \tag{13c}$$

where the notation is standard. We can rewrite eqns. (13) as follows:

$$\frac{|\mu_m|}{\Delta x_i}\left(\psi_{mout,i}^{l+1/2} - \psi_{min,i}^{l+1/2}\right) + \sigma_i \psi_{mi}^{l+1/2} = \sigma_{si}\,\phi_{oi}^{l} + q_{mi} \tag{14a}$$

$$\psi_{mi}^{l+1/2} = \frac{1}{2}\left(\psi_{mout,i}^{l+1/2} + \psi_{min,i}^{l+1/2}\right) \tag{14b}$$

$$\phi_{oi}^{l+1/2} = \sum_{m=1}^{M} w_m\,\psi_{mi}^{l+1/2} \tag{14c}$$

where

$$\psi_{mout,i}^{l+1/2} = \begin{cases} \psi_{mi+1/2}^{l+1/2}, & \mu_m > 0, \\ \psi_{mi-1/2}^{l+1/2}, & \mu_m < 0, \end{cases}$$

$$\psi_{min,i}^{l+1/2} = \begin{cases} \psi_{mi-1/2}^{l+1/2}, & \mu_m > 0, \\ \psi_{mi+1/2}^{l+1/2}, & \mu_m < 0. \end{cases}$$

Equations (14) are easily manipulated into the form used above in our general derivation:

$$\phi_{oi}^{l+1/2} = T_v^{\,i}\,\phi_{oi}^{l} + T_b^{\,i}\,\underline{\psi}_{in,i}^{l+1/2} + s_{vi} \tag{15a}$$

$$\underline{\psi}_{out,i}^{l+1/2} = R_v^{\,i}\,\phi_{oi}^{l} + R_b^{\,i}\,\underline{\psi}_{in,i}^{l+1/2} + \underline{s}_{bi} \tag{15b}$$

where

$$T_v^{\,i} = c_i \sum_{m=1}^{M} w_m \frac{\varepsilon_{mi}}{2 + \varepsilon_{mi}} \qquad (T_v^{\,i} \text{ is a 1 x 1 matrix}),$$

$$[T_b^{\,i}]_{1,m} = \frac{2w_m}{2 + \varepsilon_{mi}} \qquad (T_b^{\,i} \text{ is a 1 x M matrix}),$$

$$s_{vi} = \frac{1}{\sigma_i} \sum_{m=1}^{M} w_m \frac{\varepsilon_{mi}\,q_{mi}}{2 + \varepsilon_{mi}},$$

$$[R_v^{\,i}]_{m,1} = \frac{2\,c_i\,\varepsilon_{mi}}{2 + \varepsilon_{mi}} \qquad (R_v^{\,i} \text{ is an M x 1 matrix}),$$

$$[R_b^{\,i}]_{m,m} = \frac{2 - \varepsilon_{mi}}{2 + \varepsilon_{mi}} \qquad (R_b^{\,i} \text{ is a diagonal M x M matrix}),$$

$$[s_{bi}]_m = \frac{2\,\varepsilon_{mi}\,q_{mi}}{\sigma_i\,(2 + \varepsilon_{mi})},$$

$$\varepsilon_{mi} = \frac{\sigma_i\,\Delta x_i}{|\mu_m|},$$

$$c_i \qquad = \sigma_{si} \ / \sigma_i \, .$$

Before deriving acceleration equations from eqns. (15), we must choose the coarse angular mesh, which we will impose at cell boundaries, and create projection matrices. For our first example we choose a "double-P_0" (DP0) approximation -- in the low-order equations the angular flux on cell boundaries is represented by a constant in each angular half-space:

$$J_{i+1/2}(\mu) \quad = \quad \begin{cases} J_{+i+1/2} \, , & \mu > 0 \\ J_{-i+1/2} \, , & \mu < 0 \end{cases} \tag{16}$$

Our next task is to determine projection matrices $P_{c\leftarrow f}$ and $P_{f\leftarrow c}$ which will connect the coarse- and fine-mesh function spaces as follows:

$$J_{+i+1/2} \qquad = \sum_{\mu_m>0} [P_{c\leftarrow f}]_{1,m} \, \psi_{mi+1/2} \tag{17a}$$

$$\psi_{mi+1/2} \qquad = [P_{f\leftarrow c}]_{m,1} \, J_{+i+1/2} \; + \; \psi_{res,m,i+1} \qquad , \mu_m > 0 \tag{17b}$$

(Analagous relations hold for $\mu_m < 0$.) We consider first the coarse-to-fine projection. Since the coarse-mesh flux is a constant in each half-space, it makes sense to let the coarse-to-fine projection of that flux be the same constant. That is, we choose:

$$[P_{f\leftarrow c}]_{m,1} \quad = \quad 1, \quad \mu_m > 0, \tag{18}$$

The fine-to-coarse projection is also fairly straightforward. We simply pick some characteristic of the fine-mesh flux which we think is important, and require the coarse-mesh projection to preserve that characteristic. For example, if we think partial currents are important we will require:

$$\sum_{\mu_n>0} w_n \mu_n^k \quad \left[\sum_{\mu_m>0} [P_{c\leftarrow f}]_{1,m} \, \psi_{mi+1/2} \right] \quad = \sum_{\mu_m>0} w_m \mu_m^k \, \psi_{mi+1/2} \tag{19}$$

with k=1. This implies that

$$[P_{c\leftarrow f}]_{1,m} \quad = \quad \frac{w_m \mu_m^k}{\sum_{\mu_n>0} w_n \mu_n^k}, \quad \mu_m \; > 0, \tag{20}$$

again with k=1. If on the other hand we believe half-range *fluxes* are more important than half-range *currents*, we can choose k=0 in equations (19) and (20), giving a different projection matrix and therefore a different acceleration method.

Once we have chosen the projection matrices we are ready to proceed with the 4-step procedure described in Section II. Step 1 involves the actual projection, which gives eqns. (8). Step 2, defining

acceleration equations, gives eqns. (9). Step 3, subtracting the accelerated equations from the unaccelerated equations, gives

$$f_{oi}^{l+1} = T_v^i (\phi_{oi}^{l+1} - \phi_{oi}^{l}) + [T_b^i P^i_{f\leftarrow c}] \underline{b}_{in,i}^{l+1} \tag{21a}$$

$$\underline{b}_{out,i}^{l+1} = [P^i_{c\leftarrow f} R_v^i] (\phi_{oi}^{l+1} - \phi_{oi}^{l}) + [P^i_{c\leftarrow f} R_b^i P^i_{f\leftarrow c}] \underline{b}_{in,i}^{l+1} \tag{21b}$$

where

$$f_{oi}^{l+1} \equiv \phi_{oi}^{l+1} - \phi_{oi}^{l+1/2} ,$$

$$\underline{b}_{in,i}^{l+1} \equiv [b_{+i-1/2}^{l+1} , b_{-i+1/2}^{l+1}]^t ,$$

$$\underline{b}_{out,i}^{l+1} \equiv [b_{+i+1/2}^{l+1} , b_{-i-1/2}^{l+1}]^t ,$$

$$b_{\pm,i+1/2}^{l+1} \equiv J_{\pm,i+1/2}^{l+1} - J_{\pm,i+1/2}^{l+1/2} ,$$

$$T_v^i = c_i \sum_{m=1}^{M} w_m \frac{\varepsilon_{mi}}{2+\varepsilon_{mi}} ,$$

$$[T_b^i P^i_{f\leftarrow c}] = \left[\sum_{\mu_m>0} \frac{2 w_m}{2+\varepsilon_{mi}} , \sum_{\mu_m<0} \frac{2 w_m}{2+\varepsilon_{mi}} \right] ,$$

$$[P_{c\leftarrow f} R_v]^i = \left[\frac{c_i}{\alpha_+} \sum_{\mu_m>0} \frac{2 w_m \mu_m^k \varepsilon_{mi}}{2+\varepsilon_{mi}} , \frac{c_i}{\alpha_-} \sum_{\mu_m<0} \frac{2 w_m |\mu_m|^k \varepsilon_{mi}}{2+\varepsilon_{mi}} \right]^t ,$$

$$[P^i_{c\leftarrow f} R_b^i P^i_{f\leftarrow c}] = \mathrm{diag}\left[\frac{c_i}{\alpha_+} \sum_{\mu_m>0} \frac{w_m \mu_m^k (2-\varepsilon_{mi})}{2+\varepsilon_{mi}} , \frac{c_i}{\alpha_-} \sum_{\mu_m<0} \frac{w_m |\mu_m|^k (2-\varepsilon_{mi})}{2+\varepsilon_{mi}} \right] ,$$

$$\alpha_+ = \sum_{\mu_n>0} w_n \mu_n^k ,$$

$$\alpha_- = \sum_{\mu_n<0} w_n |\mu_n|^k ,$$

It is a simple matter to eliminate f_{oi} from equations (21) to obtain an equation for the interface quantities $b_{in/out,i}$ (see equation (12)). In slab geometry, the resulting system can be put into tridiagonal form which can be efficiently solved by LU decomposition with forward and back substitution; this was the method used to generate the numerical results shown in the next section.

As a second example, we choose "double-P_1" (DP1) for our coarse-mesh function space. That is, in the low-order equations the angular flux on cell boundaries is represented by a linear function in each angular half-space:

$$J_{i+1/2}(\mu_m) = \begin{cases} J_{0+,i+1/2}\,P_0(2\mu_m - 1) + J_{1+,i+1/2}\,P_1(2\mu_m - 1)\ , & \mu_m > 0 \\ J_{0-,i+1/2}\,P_0(2\mu_m + 1) + J_{1-,i+1/2}\,P_1(2\mu_m + 1)\ , & \mu_m < 0 \end{cases} \tag{22}$$

where $P_n(x)$ is the nth Legendre polynomial.

Our next task is to determine projection matrices $P_{c\leftarrow f}$ and $P_{f\leftarrow c}$ which will connect the coarse- and fine-mesh function spaces as follows:

$$J_{0+i+1/2} = \sum_{\mu_m>0} [P_{c\leftarrow f}]_{1,m}\,\Psi_{mi+1/2} \tag{23a}$$

$$J_{1+i+1/2} = \sum_{\mu_m>0} [P_{c\leftarrow f}]_{2,m}\,\Psi_{mi+1/2} \tag{23b}$$

$$\Psi_{mi+1/2} = [P_{f\leftarrow c}]_{m,1}\,J_{0+i+1/2} + [P_{f\leftarrow c}]_{m,2}\,J_{1+i+1/2} + \Psi_{res,m,i+1}\ , \quad \mu_m > 0 \tag{23c}$$

(Analagous relations hold for $\mu_m < 0$.) Again we choose a simple form for the coarse-to-fine matrix $P_{f\leftarrow c}$, based on eqns. (22) and (23c):

$$[P_{f\leftarrow c}]_{m,1} = P_0(2\mu_m - 1), \quad \mu_m > 0, \tag{24a}$$

$$[P_{f\leftarrow c}]_{m,2} = P_1(2\mu_m - 1), \quad \mu_m > 0. \tag{24b}$$

The fine-to-coarse projection $P_{f\leftarrow c}$ is obtained, as it was in the DP0 case, by choosing some important characteristics of the fine-mesh flux and requiring that the coarse-mesh flux retain them. For example, if we believe that half-range angular moments are important we might require:

$$\sum_{\mu_n>0} w_n \mu_n^{k(j)}\,J_{i+1/2}(\mu_n) = \sum_{\mu_m>0} w_m \mu_m^{k(j)}\,\Psi_{mi+1/2}\ , \ j = 1 \text{ and } 2, \tag{25a}$$

where $$J_{i+1/2}(\mu_n) = J_{0+,i+1/2}\,P_0(2\mu_n - 1) + J_{1+,i+1/2}\,P_1(2\mu_n - 1)\ , \ \mu_n > 0, \tag{25b}$$

with k(j) determining which half-range moments are to be preserved under the projection. (For example, if we think it best to preserve half-range currents and fluxes, we can let k(1) = 0 and k(2) = 1. If we prefer odd half-range moments, we let k(1) = 1 and k(2) = 3.) Equations (25) can be compactly written as follows:

$$A\,\underline{J}_{+i+1/2} = B\,\underline{\Psi}_{+i+1/2}\ , \tag{26}$$

where $A_{jl} = \sum_{\mu_n>0} w_n \mu_n^{k(j)} P_{l-1}(2\mu_n - 1)$ (a 2 x 2 matrix),

$B_{jm} = w_m \mu_m^{k(j)}\ , \ \mu_m > 0$ (a 2 x [M/2] matrix),

$$\underline{J}_{+i+1/2} = [\, J_{0+,i+1/2}\,,\, J_{1+,i+1/2}\,]^t\,,$$

$$\underline{\Psi}_{+i+1/2} = \mathrm{col}[\, \psi_{mi+1/2}\,],\ \mu_m>0.$$

This implies that

$$[P_{c\leftarrow f}]_{j,m} = [A^{-1}B]_{j,m}\,,\ j=1 \text{ or } 2,\ \mu_m > 0. \tag{27}$$

Once the projection matrices $P_{c\leftarrow f}$ and $P_{f\leftarrow c}$ are determined, we proceed with the four-step procedure to arrive at low-order equations for the interface quantities $\underline{b}_{i+1/2}$ exactly as before.

To summarize, projection matrices are obtained by first deciding how many unknowns will be used to describe the coarse-mesh angular flux (i.e., determining the coarse-mesh function space), then stating mathematically which characteristics of the fine-mesh (high-order) flux will be retained by the coarse-mesh (low-order) flux. The success of the resulting acceleration scheme will depend on how well the low-order equations approximate the high-order equations, which in turn depends on which characteristics are "preserved" by the projections.

IV. SLAB GEOMETRY ANALYSIS AND NUMERICAL RESULTS

Thus far we have demonstrated that "acceleration" equations can be derived, for virtually any transport differencing scheme regardless of geometry or mesh shape, by using a "coarse-mesh" angular flux approximation on cell boundaries. We have given the details of this derivation for two particular cases. However, we have yet to show that the "acceleration" equations so derived will actually accelerate the transport iteration.

In this section we present results from a Fourier analysis of a simple model problem (infinite medium, constant mesh spacing, constant cross section, isotropic scattering) for various discretization schemes and two different BPA methods. The Fourier analysis method is taken from Larsen[5], although the procedural details used here are somewhat different (and considerably simpler). We also present numerical results from a model-like problem which confirm the predictions of the analysis. Finally, we present numerical results from a non-model-like problem which agree with the observation made by previous researchers: despite the fact that the analysis is rigorously valid only for the model problem, its predictions appear to hold for all problems[14,15].

A. Fourier Analysis

We begin with the discretized transport equation (6), rewritten here for slab geometry in a slightly different form:

$$\underline{\Phi}_{oi}^{l+1/2} = T_v\, \underline{\Phi}_{oi}^{l} + T_{b+}\, \underline{\Psi}_{+i-1/2}^{l+1/2} + T_{b-}\, \underline{\Psi}_{-i+1/2}^{l+1/2} + \underline{s}_{vi} \tag{28a}$$

$$\underline{\Psi}_{+i+1/2}^{l+1/2} = R_{v+}\, \underline{\Phi}_{oi}^{l} + R_{b+}\, \underline{\Psi}_{+i-1/2}^{l+1/2} + \underline{s}_{b+i} \tag{28b}$$

$$\underline{\Psi}_{-i-1/2}^{l+1/2} = R_{v-}\,\underline{\phi}_{oi}^{l} + R_{b-}\,\underline{\Psi}_{-i+1/2}^{l+1/2} + \underline{s}_{b-i} \tag{28c}$$

where we have separated the boundary angular fluxes into right-directed ('+' subscript) and left-directed ('–' subscript) vectors, and split the matrices accordingly. (Note that if we assume material properties are constant, as will be necessary for our model problem analysis, we may write the T and R matrices without cell indices *i*.) Equations (28) hold for virtually any slab-geometry transport differencing scheme, and the same will be true of the Fourier analysis performed here.

Given eqns. (28) as our starting point, the first 3 steps of our 4-step BPA procedure will give the following:

$$\underline{f}_{oi}^{l+1} = T_v\,(\underline{\phi}_{oi}^{l+1} - \underline{\phi}_{oi}^{l}) + [T_{b+}{}^{i}P_{f\leftarrow c+}]\,\underline{b}_{+i-1/2}^{l+1} + [T_{b-}{}^{i}P_{f\leftarrow c-}{}^{i}]\,\underline{b}_{-i+1/2}^{l+1} \tag{29a}$$

$$\underline{b}_{+i+1/2}^{l+1} = [P_{c\leftarrow f+}\,R_{v+}]\,(\underline{\phi}_{oi}^{l+1} - \underline{\phi}_{oi}^{l}) + [P_{c\leftarrow f+}\,R_{b+}\,P_{f\leftarrow c+}]\,\underline{b}_{+i-1/2}^{l+1} \tag{29b}$$

$$\underline{b}_{-i-1/2}^{l+1} = [P_{c\leftarrow f-}\,R_{v-}]\,(\underline{\phi}_{oi}^{l+1} - \underline{\phi}_{oi}^{l}) + [P_{c\leftarrow f-}\,R_{b-}\,P_{f\leftarrow c-}]\,\underline{b}_{+i+1/2}^{l+1} \tag{29c}$$

where $\underline{f}_{oi}^{l+1} = \underline{\phi}_{oi}^{l+1} - \underline{\phi}_{oi}^{l+1/2}$.

To begin the analysis, we propose the following Fourier ansatz:

$$(\underline{\phi}_{oi}^{l+1/2} - \underline{\phi}_{oi}^{l-1/2}) = \omega^{l}\,\underline{A}\,e^{j\lambda x_i}\,, \qquad j \equiv \sqrt{-1}, \tag{30a}$$

$$(\underline{\Psi}_{\pm i+1/2}^{l+1/2} - \underline{\Psi}_{\pm i+1/2}^{l-1/2}) = \omega^{l}\,\underline{a}_{\pm}\,e^{j\lambda x_{i+1/2}}\,, \tag{30b}$$

$$(\underline{\phi}_{oi}^{l} - \underline{\phi}_{oi}^{l-1}) = \omega^{l}\,\underline{B}\,e^{j\lambda x_i}\,, \tag{30c}$$

$$(\underline{b}_{\pm i+1/2}^{l+1} - \underline{b}_{\pm i+1/2}^{l}) = \omega^{l}\,\underline{d}_{\pm}\,e^{j\lambda x_{i+1/2}}\,, \tag{30d}$$

Our objective is to find an expression for the eigenvalue ω as a function of the Fourier parameter λ. If we subtract successive iterates of eqns. (28) and introduce our ansatz into the result, we obtain

$$\underline{A} = T_v\,\underline{B} + T_{b+}\,\underline{a}_{+}\,e^{-j\lambda h/2} + T_{b-}\,\underline{a}_{-}\,e^{j\lambda h/2}\,, \tag{31a}$$

$$\underline{a}_{+}\,e^{j\lambda h/2} = R_{v+}\,\underline{B} + R_{b+}\,\underline{a}_{+}\,e^{-j\lambda h/2}\,, \tag{31b}$$

$$\underline{a}_{-}\,e^{-j\lambda h/2} = R_{v-}\,\underline{B} + R_{b-}\,\underline{a}_{-}\,e^{j\lambda h/2}\,, \tag{31c}$$

where h is the (constant) mesh spacing $x_{i+1/2} - x_{i-1/2}$. These equations are easily solved for $\underline{A}$:

$$\underline{A} = X\,\underline{B} \tag{32}$$

where $X = \{\, T_v + T_{b+}[\varepsilon I - R_{b+}]^{-1}R_{v+} + T_{b-}[\,\bar{\varepsilon} I - R_{b-}]^{-1}\,R_{v-}\,\}$,

$$\varepsilon = e^{j\lambda h},$$

$$\bar{\varepsilon} = e^{-j\lambda h}.$$

Similarly, if we subtract successive iterates of eqns. (29) and insert the ansatz we obtain

$$(\omega \underline{B} - \underline{A}) = T_v (\omega - 1)\, \underline{B} + [T_{b+} P_{f\leftarrow c+}]\, \underline{d}_+ e^{-j\lambda h/2} + [T_{b-} P_{f\leftarrow c-}]\, \underline{d}_- e^{j\lambda h/2}, \quad (33a)$$

$$\underline{d}_+ e^{j\lambda h/2} = [P_{c\leftarrow f+} R_{v+}]\, (\omega - 1)\, \underline{B} + [P_{c\leftarrow f+} R_{b+} P_{f\leftarrow c+}]\, \underline{d}_+ e^{-j\lambda h/2}, \quad (33b)$$

$$\underline{d}_- e^{-j\lambda h/2} = [P_{c\leftarrow f-} R_{v-}]\, (\omega - 1)\, \underline{B} + [P_{c\leftarrow f-} R_{b-} P_{f\leftarrow c-}]\, \underline{d}_- e^{j\lambda h/2}, \quad (33c)$$

which is easily manipulated to yield:

$$(\omega \underline{B} - \underline{A}) = (\omega - 1)\, Z\, \underline{B}, \quad (34)$$

where $Z = \{T_v + [T_{b+} P_{f\leftarrow c+}][\varepsilon I - (P_{c\leftarrow f+} R_{b+} P_{f\leftarrow c+})]^{-1} [P_{c\leftarrow f+} R_{v+}] + [T_{b-} P_{f\leftarrow c-}][\bar{\varepsilon} I - (P_{c\leftarrow f-} R_{b-} P_{f\leftarrow c-})]^{-1} [P_{c\leftarrow f-} R_{v-}]\}.$

Substituting equation (32) into equation (34) gives our desired result:

$$[I - Z]^{-1} [X - Z]\, \underline{B} = \omega\, \underline{B}. \quad (35)$$

That is, ω is actually the set of eigenvalues of the matrix $[I - Z]^{-1}[X - Z]$. Note that the matrices Z and X, and hence the eigenvalues ω, depend on the parameter $\theta \equiv \lambda h$.

We have written a computer code which performs the above analysis for virtually arbitrary spatial discretization schemes for the (slab-geometry) discrete-ordinates transport equation. For any given value of h and any given quadrature, the code performs a search, over all $\theta \in (0,2\pi)$ and all $c \in [0,1)$, for the maximum eigenvalue, which is termed the *spectral radius* for that mesh size and quadrature. The code accepts from a subroutine the "T" and "R" matrices which appear in the above formulas; the projection matrices $P_{c\leftarrow f}$ and $P_{f\leftarrow c}$ are provided by another subroutine. Thus, performing the analysis for a given spatial discretization simply involves plugging in the subroutine which gives the "T" and "R" matrices for that discretization. Likewise, performing the analysis for any particular BPA scheme simply involves plugging in the appropriate projection-matrix subroutine.

We have performed this analysis for the diamond differencing[27] (DD), step differencing[14] (SD), linear discontinuous[27] (LD), and linear moments[28] (LM) spatial discretization schemes, for both the "double-P_0" (DP0) and "double-P_1" (DP1) acceleration methods which were described in Section III. The results are summarized in Tables I and II and Figures I-IV. Table I gives the maximum value of ω/c over all $h \in (0,\infty)$, $c \in [0,1)$, and $\theta \in (0,2\pi)$, as a function of quadrature order, for three different DP0 projections. (Standard Gauss-Legendre quadrature sets were used.) Table II gives the

same information for four different DP1 projections, for standard quadratures (S_N) as well as "double" quadratures (DS_N). For every method, every mesh size, and every quadrature, the maximum value of ω/c occurred at c=1.

The first DP0 method shown in Table I preserves half-range fluxes (i.e., the weighting function in each half-range integral was $\mu^0 = 1$); the second preserves partial currents (weighting function = μ^1); the third preserves a combination of half-range first and second moments (weighting function = $\mu + \sqrt{3}\cdot\mu^2$). It is clear that the method chosen for projection makes a significant difference: the 0th-moment method is unstable, the first-moment method gives $\omega < c/3$, and the combination method gives $\omega < 0.2247c$ for all but the DD discretization. This serves to illustrate two points. First, the BPA method is quite flexible -- even after the coarse angular mesh is chosen, there is an unlimited variety of projections which can be used to produce low-order equations. Second, it is probably not possible to produce the *optimal* projection by inspection or intuition; instead, we must experiment a bit (here the Fourier analysis is an invaluable tool). (Incidentally, the 'combination' method arose from requiring that the DP0 acceleration perform exactly like DSA in the fine-mesh limit.)

Table I. Spectral Radius of Simple Slab-Geometry DP0 Schemes as a Function of Quadrature Order: Various Projections.

Quad-rature	Half-range moment preserved (weighting function)					
	0th (1.0)		1st (μ)		Combination ($\mu + \sqrt{3}\,\mu^2$)	
	LD, LM, and SD	DD	LD, LM, and SD	DD	LD, LM, and SD	DD
S2	0	0	0	0	0	0
S4	.7974	.7974	.2268	.2268	.1848	.331
S8	1.918	1.918	.3031	.3031	.2224	.399
S16	3.373	3.373	.3253	.3253	.2247	.417
S32	5.163	5.163	.3313	.3313	.2247	.421

The DP1 methods (Table II) have *two* low-order angular unknowns per half-space; hence two "characteristics" of the fine-mesh flux can be "preserved". We again chose half-range moments, and experimented with four different combinations: 0th and 1st, 0th and 2nd, 1st and 2nd, and 1st and 3rd. Again, the method of projection (i.e., the chosen combination of moments) makes a difference in performance, although all four methods appear to be stable and rapidly convergent.

Figures I-IV give $\rho \equiv (\omega/c)_{max}$, vs. mesh size for the LD, LM, SD, and DD discretizations. Each figure has analysis results from Larsen's DSA scheme, a DP0 method, and a DP1 method. Also, Figure I contains numerical estimates of the spectral radius from a model-like problem (see Section B below). All curves are for the S_{16} quadrature. The most striking feature of the BPA curves is that, with the exception of the anomalous diamond-differenced (DD) case, the spectral radius monotonically decreases with increasing mesh size. Intuitively, this is understandable since the low-order

approximation takes place only on cell boundaries, and as the boundaries get farther apart they become relatively less important. For example, as the mesh size increases the exiting flux from a region depends more and more on the interior source and less on streaming from the opposite boundary. The DD behavior is explainable by noting that for large meshes, "streaming" from the opposite boundary begins to *dominate* rather than die out (the surface-to-surface transfer coefficients approach –1 instead of 0).

Table II. Spectral Radius of Simple Slab-Geometry DP1 Schemes as a Function of Quadrature Order: Various Projections.

Quad-rature	Half-range moments preserved (weighting functions)							
	0th, 1st (1.0, μ)		0th, 2nd (1.0, μ^2)		1st, 2nd (μ, μ^2)		1st, 3rd (μ, μ^3)	
	LD, LM, SD	DD	LD, LM, SD	DD	LD, LM, SD	DD	LD, LM, SD	DD
S4	0	0	0	0	0	0	0	0
S6	.0063	.0100	.0120	.0166	.0100	.043	.0166	.063
S8	.0151	.0215	.0268	.0320	.0215	.073	.0320	.095
S16	.0431	.0460	.0689	.0689	.0460	.111	.0586	.130
S32	.0700	.0700	.1068	.1068	.0550	.121	.0657	.140
DS2	0	0	0	0	0	0	0	0
DS3	.0348	.0503	.0616	.0666	.0503	.125	.0666	.143
DS4	.0624	.0609	.0987	.0987	.0609	.125	.0730	.143
DS8	.1047	.1047	.1546	.1546	.0551	.125	.0654	.143
DS16	.1324	.1324	.1943	.1943	.0553	.125	.0656	.143

Figure I. Spectral Radius vs. Mesh Size, LD, S-16.

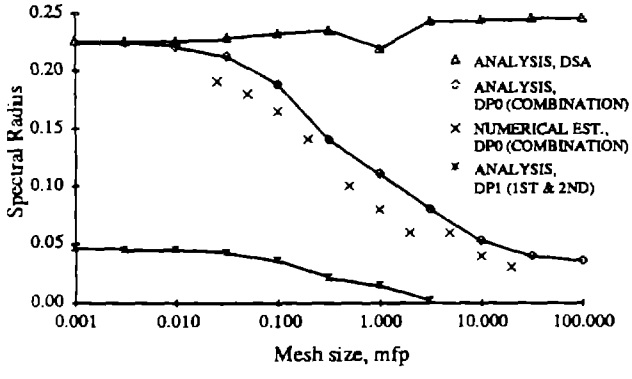

Figure II. Spectral Radius vs. Mesh Size, LM, S-16.

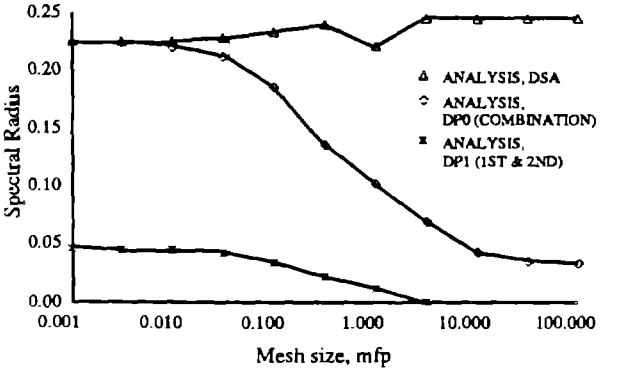

Figure III. Spectral Radius vs. Mesh Size, SD, S-16.

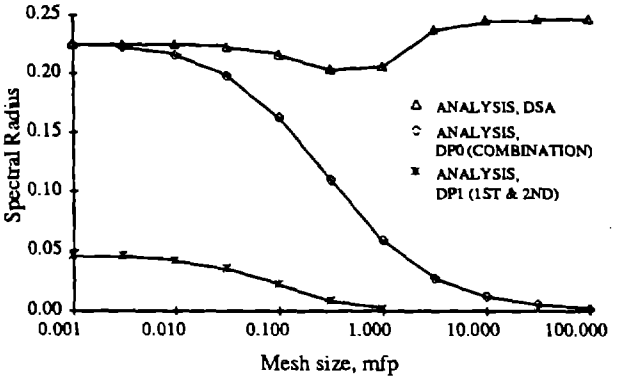

Figure IV. Spectral Radius vs. Mesh Size, DD, S-16.

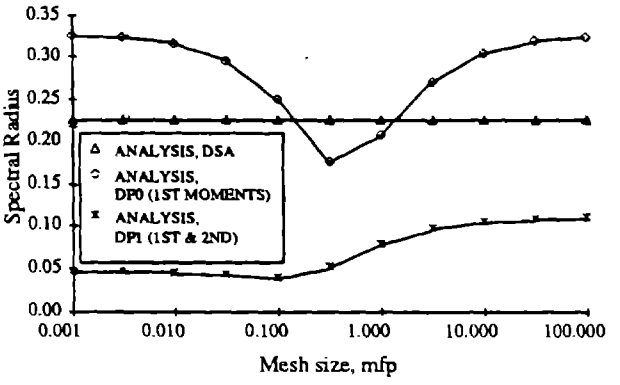

B. Numerical Results

Calculations were performed on a model-like problem (80 mean-free path homogeneous slab with vacuum boundaries, c=1, constant cross-sections, isotropic scattering, source = 1 in some meshes and 0 in others) in an attempt to verify that the Fourier analysis described above had been coded correctly. The DP0 BPA method was used to accelerate an LD discrete-ordinates code, and the following spectral radius estimate was calculated at each iteration:

$$\rho \approx \frac{\| \phi_o^{l+1} - \phi_o^{l} \|_2}{\| \phi_o^{l} - \phi_o^{l-1} \|_2} , \tag{36}$$

where $\| \ \|_2$ indicates the L_2 norm:

$$\| \underline{f} \|_2 = [\sum_i f_i^2]^{1/2} , \tag{37}$$

Results from this numerical estimate of the spectral radius are plotted along with the analysis predictions in Figure I. Agreement is good, leading us to conclude that the analysis was performed and encoded correctly.

Since the analysis is strictly valid only for the model problem, we have also performed numerical calculations (and ρ estimates) using a number of non-model-like problems. One of these is shown in Figure V, and the results are summarized in Table III. In each case the numerically-estimated spectral radius is lower than that predicted by the analysis; the same has been observed on many other problems not shown here. Moreover, this has been observed by other researchers using different numerical methods: the predictions of the model-problem analysis are remarkably accurate even for complicated problems with varying mesh widths and cross-sections[14,15]. Finally, we note that numerical results obtained by Lawrence, using his DP0 method (a partial-current preserver) with the DD and LM schemes, are in agreement with the observations made here[19].

Figure V. Reed's Problem

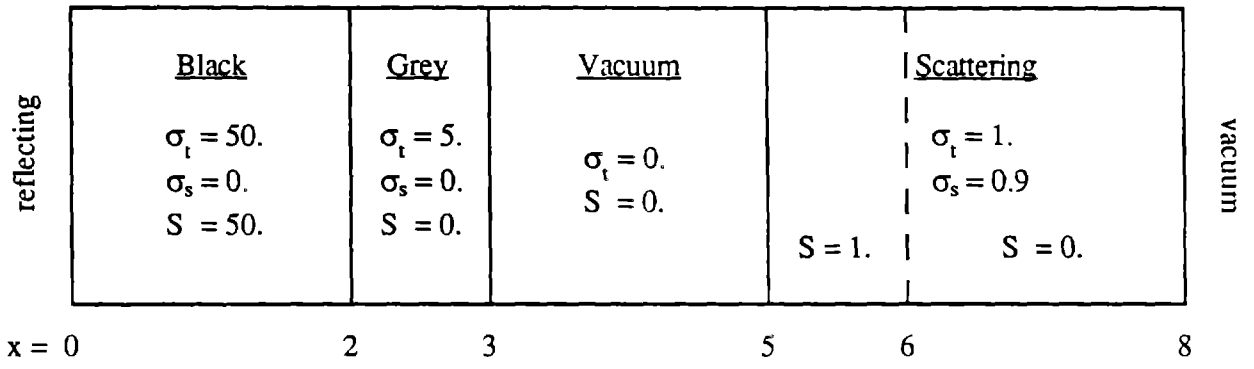

Table III. Numerical Estimates ofSpectral Radius vs. Mesh Size: Reed's Problem

Mesh Size, cm (mfp)					Iterations	Estimated
Black	Grey	Vacuum	Source	Scattering	to 10^{-6}	Spec. Radius
1.0 (50)	1.0 (5)	2.0 (0)	1.0 (1.0)	1.0 (1.0)	5	0.06
0.5 (25)	0.5 (2.5)	2.0 (0)	1.0 (1.0)	1.0 (1.0)	5	0.06
0.2 (10)	0.2 (1.0)	2.0 (0)	0.5 (0.5)	0.5 (0.5)	6	0.08
0.2 (10)	0.2 (1.0)	2.0 (0)	0.1 (0.1)	1.0 (1.0)	8	0.13

V. SUMMARY & CONCLUSIONS

A class of synthetic acceleration methods has been presented which obtains low-order equations by *projecting* the transport angular flux onto a coarse mesh *only on cell boundaries*. The ultimate objective of our work is to find an acceleration method which

1) gives unconditional rapid convergence,
2) can be used regardless of geometry, mesh shape, or discretization scheme,
3) has easily-solved low-order equations, and
4) gives a converged solution identical to the unaccelerated solution.

We have shown that the new BPA methods are general with respect to geometry, mesh shape, and discretization scheme, and that they give a solution identical to the unaccelerated solution. The question of rapid convergence has been answered affirmatively, but only for slab geometry, in which the simplest BPA method (DP0) was shown to give a spectral radius (ρ) bounded by c/3. We have presented no results in higher geometries; however, we can argue that there exist BPA methods such that unconditional rapid convergence can be attained in any geometry. As a trivial example, note that immediate convergence (ρ=0) is obtained by using a "coarse" angular mesh which is identical to the transport angular mesh.

The remaining question is whether the low-order equations of a rapidly-convergent BPA method can be solved efficiently. The equations are easily put into a form amenable to solution via iteration on interface unknowns, but two things remain to be shown. First, the iteration on the low-order interface unknowns must be shown to converge reasonably quickly, or else be amenable to some sort of acceleration itself. Second, the number of low-order interface unknowns must be reasonably small (which of course eleminates the trivial example cited above). We note that numerical results obtained by Lawrence[19] using his DP0 method (only two angular unknowns per spatial unknown per cell interface) in two and three dimensions are encouraging: not only was the accelerated iteration count very low, but the red/black iterative scheme used to solve the low-order equations was reasonably efficient. However, these results are from a limited set of test problems; further study is necessary before any BPA scheme can be declared generally useful in two or three dimensions. Therefore, we are analyzing the low-order iteration in XY geometry, and investigating the possibility of using multigrid methods to accelerate it. We are also studying the question of how many low-order interface unknowns are needed to produce a generally effective BPA scheme in XY geometry.

APPENDIX: FOUR-STEP BPA PROCEDURE -- THE GENERAL CASE

In Section II a four-step BPA derivation was presented which was general with respect to geometry and mesh shape, and essentially general with respect to discretization scheme. However, it contained the assumption that the coarse-mesh boundary unknowns associated with each cell could be divided into two distinct sets: one set which depended only on the incoming angular flux and another which depended only on the outgoing angular flux. In this appendix we present the same derivation with that assumption removed.

As before, we begin with the discretized transport equation written in first-flight response matrix form:

$$\underline{\Phi}_{oi}^{l+1/2} = T_v^i \underline{\Phi}_{oi}^{l} + T_b^i \underline{\Psi}_{in,i}^{l+1/2} + \underline{S}_{v,i} \tag{A.1a}$$

$$\underline{\Psi}_{out,i}^{l+1/2} = R_v^i \underline{\Phi}_{oi}^{l} + R_b^i \underline{\Psi}_{in,i}^{l+1/2} + \underline{S}_{b,i} \tag{A.1b}$$

with

$$\underline{\Psi}_{in,i}^{l+1/2} = \sum_{j\,@\,i} H_{i\leftarrow j}\, \underline{\Psi}_{out,j}^{l+1/2} \ , \tag{A.2}$$

where $H_{i\leftarrow j}$ = renumbering matrix which extracts the incoming flux to cell i from the outgoing flux of the adjacent cell j,

$\sum_{j\,@\,i}$ = sum over all cells j which are adjacent to cell i.

As before we will define a vector of coarse-mesh boundary unknowns, and projection matrices which take us back and forth between fine- and coarse-mesh function spaces, but here it is convenient to define them a bit differently. First we note that

$$H_{i\leftarrow j}\,\Psi_{out,j}^{l+1/2} = \text{angular flux leaving cell } j \text{ and entering cell } i,$$
$$H_{j\leftarrow i}\,\Psi_{out,i}^{l+1/2} = \text{angular flux leaving cell } i \text{ and entering cell } j.$$

Then we define our coarse-mesh boundary flux $\underline{J}_{ij}$ on the surface between cells i and j as a projection of the above two quantities:

$$\underline{J}_{ij}^{l+1/2} \equiv \underline{J}_{ji}^{l+1/2} = P_{c\leftarrow f,j\leftarrow i}\,[H_{j\leftarrow i}\,\Psi_{out,i}^{l+1/2}] + P_{c\leftarrow f,i\leftarrow j}\,[H_{i\leftarrow j}\,\Psi_{out,j}^{l+1/2}], \tag{A.3}$$

where $P_{c\leftarrow f,j\leftarrow i}$ = fine-to-coarse projection matrix for the surface between cells i and j; gives contribution to coarse-mesh vector from the fine-mesh flux going from cell i to cell j,

$P_{c\leftarrow f,i\leftarrow j}$ = fine-to-coarse projection matrix for the surface between cells i and j; gives contribution to coarse-mesh vector from the fine-mesh flux going from cell j to cell i.

If we define the following shorthand notation,

$$[PH]_{j\leftarrow i} \equiv P_{c\leftarrow f,j\leftarrow i}\,H_{j\leftarrow i}\,,$$
$$[PH]_{i\leftarrow j} \equiv P_{c\leftarrow f,i\leftarrow j}\,H_{i\leftarrow j}\,,$$

then we can write eqn. (A.3) as follows:

$$\underline{J}_{ij}^{l+1/2} \equiv \underline{J}_{ji}^{l+1/2} = [PH]_{j\leftarrow i}\,\Psi_{out,i}^{l+1/2} + [PH]_{i\leftarrow j}\,\Psi_{out,j}^{l+1/2}, \tag{A.4}$$

Note that the coarse-mesh unknowns are no longer subject to the restriction imposed in Section II.

As before, we define an incoming flux residual for each cell i:

$$\Psi_{res,i}^{l+1/2} = \Psi_{in,i}^{l+1/2} - \sum_{j\,@\,i} P_{i\leftarrow ij}\;\underline{J}_{ij}^{l+1/2}\,, \tag{A.5}$$

where $P_{i\leftarrow ij}$ = coarse-to-fine "projection" matrix giving the coarse-mesh approximation to the fine-mesh angular flux entering cell i from cell j.

We are now ready to proceed with the four-step procedure.

Step 1 -- project onto coarse mesh. This simply involves making use of the above definitions and operating on the discretized transport equation (A.1). The result is:

$$\underline{\Phi}_{o,i}^{l+1/2} = T_v^i \underline{\Phi}_{o,i}^{l} + T_b^i [\underline{\Psi}_{res,i}^{l+1/2} + \sum_{k @ i} P_{i \leftarrow ik} \underline{J}_{ik}^{l+1/2}] + \underline{S}_{v,i} \qquad \text{(A.6a)}$$

$$[PH]_{j \leftarrow i} \underline{\Psi}_{out,i}^{l+1/2} = [PH]_{j \leftarrow i} R_v^i \underline{\Phi}_{o,i}^{l} + [PH]_{j \leftarrow i} R_b^i [\underline{\Psi}_{res,i}^{l+1/2} + \sum_{k @ i} P_{i \leftarrow ik} \underline{J}_{ik}^{l+1/2}] + [PH]_{j \leftarrow i} \underline{S}_{b,i} \qquad \text{(A.6b)}$$

where (A.6b) holds for all j such that cell j shares a surface with cell i.

Step 2 -- define acceleration equations. As before, this involves changing iteration indices to $l+1$ on all terms except the incoming residual:

$$\underline{\Phi}_{o,i}^{l+1} = T_v^i \underline{\Phi}_{o,i}^{l+1} + T_b^i [\underline{\Psi}_{res,i}^{l+1/2} + \sum_{k @ i} P_{i \leftarrow ik} \underline{J}_{ik}^{l+1}] + \underline{S}_{v,i} \qquad \text{(A.7a)}$$

$$[PH]_{j \leftarrow i} \underline{\Psi}_{out,i}^{l+1} = [PH]_{j \leftarrow i} R_v^i \underline{\Phi}_{o,i}^{l+1} + [PH]_{j \leftarrow i} R_b^i [\underline{\Psi}_{res,i}^{l+1/2} + \sum_{k @ i} P_{i \leftarrow ik} \underline{J}_{ik}^{l+1}] + [PH]_{j \leftarrow i} \underline{S}_{b,i} \qquad \text{(A.7b)}$$

Step 3 -- subtract (accel. eqns. – unaccel. eqns.). Subtracting eqns. (A.7) – (A.6) yields:

$$\underline{f}_{o,i}^{l+1} = T_v^i (\underline{f}_{o,i}^{l+1} + \underline{\delta\Phi}_{o,i}^{l+1/2}) + T_b^i \sum_{k @ i} P_{i \leftarrow ik} \underline{b}_{ik}^{l+1} \qquad \text{(A.8a)}$$

$$\underline{d}_{j \leftarrow i}^{l+1} = [PH]_{j \leftarrow i} R_v^i (\underline{f}_{o,i}^{l+1} + \underline{\delta\Phi}_{o,i}^{l+1/2}) + [PH]_{j \leftarrow i} R_b^i \sum_{k @ i} P_{i \leftarrow ik} \underline{b}_{ik}^{l+1} \qquad \text{(A.8b)}$$

where

$$\underline{f}_{o,i}^{l+1} \equiv \underline{\Phi}_{o,i}^{l+1} - \underline{\Phi}_{o,i}^{l+1/2},$$

$$\underline{\delta\Phi}_{o,i}^{l+1} \equiv \underline{\Phi}_{o,i}^{l+1/2} - \underline{\Phi}_{o,i}^{l+1},$$

$$\underline{d}_{j \leftarrow i}^{l+1} \equiv [PH]_{j \leftarrow i} \underline{\Psi}_{out,i}^{l+1} - [PH]_{j \leftarrow i} \underline{\Psi}_{out,i}^{l+1/2},$$

$$\underline{b}_{ij}^{l+1} \equiv \underline{J}_{ij}^{l+1} - \underline{J}_{ij}^{l+1/2} = \underline{d}_{j \leftarrow i}^{l+1} + \underline{d}_{i \leftarrow j}^{l+1} = \underline{b}_{ji}^{l+1}.$$

Step 4 -- put in form convenient for solution. We solve eqn. (A.8a) for $\underline{f}_{o,i}^{l+1}$ and insert the result into eqn. (A.8b) to obtain:

$$\underline{d}_{j\leftarrow i}^{l+1} = M_{vj\leftarrow i}\ \underline{\delta\phi}_{oi}^{l+1/2} + M_{bj\leftarrow i} \sum_{k\,@\,i} P_{i\leftarrow ik}\ \underline{b}_{ik}^{l+1}\ , \tag{A.9}$$

where

$$M_{vj\leftarrow i} \equiv [PH]_{j\leftarrow i}\, R_v^i + [PH]_{j\leftarrow i}\, R_v^i\, [I - T_v^i]^{-1}\, T_v^i\ ,$$

$$M_{bj\leftarrow i} \equiv [PH]_{j\leftarrow i}\, R_b^i + [PH]_{j\leftarrow i}\, R_v^i\, [I - T_v^i]^{-1}\, T_b^i\ .$$

Next, we write an equation identical to (A.9) except that it is for the quantity $\underline{d}_{i\leftarrow j}^{l+1}$:

$$\underline{d}_{i\leftarrow j}^{l+1} = M_{vi\leftarrow j}\ \underline{\delta\phi}_{oi}^{l+1/2} + M_{bi\leftarrow j} \sum_{k\,@\,j} P_{j\leftarrow jk}\ \underline{b}_{jk}^{l+1}\ , \tag{A.10}$$

and add eqns. (A.9) and (A.10) to obtain, finally,

$$\underline{b}_{ij}^{l+1} = M_{vj\leftarrow i}\ \underline{\delta\phi}_{oi}^{l+1/2} + M_{bj\leftarrow i} \sum_{k\,@\,i} P_{i\leftarrow ik}\ \underline{b}_{ik}^{l+1}\ ,$$

$$+ M_{vi\leftarrow j}\ \underline{\delta\phi}_{oj}^{l+1/2} + M_{bi\leftarrow j} \sum_{k\,@\,j} P_{j\leftarrow jk}\ \underline{b}_{jk}^{l+1}\ , \tag{A.11}$$

Equation (A.11) can presumably be solved by iteration on the interface quanties $\underline{b}_{ij}^{l+1}$, after which eqn. (A.8a) can be invoked to give the scalar-flux corrections $\underline{f}_{oi}^{l+1}$.

ACKNOWLEDGEMENTS

We thank E. W. Larsen and R. D. Lawrence for a number of helpful discussions and comments, and R. D. Lawrence for sharing his numerical results.

Part of this work was performed under M. L. Adams's appointment to the Nuclear Engineering, Health Physics, and Radioactive Waste Management Fellowship program administered by Oak Ridge Associated Universities for the U. S. Department of Energy, in partial fulfillment of the requirements for the Ph.D degree at The University of Michigan.

REFERENCES

1. W. A. Rhoades and F. R. Mynatt, "The DOT-III Two-Dimensional Discrete Ordinates Transport Code", ORNL-TM-4280, Oak Ridge National Laboratory (1973).

2. T. J. Seed, W. F. Miller, Jr., and F. W. Brinkley, Jr., "TRIDENT: A Two-Dimensional Multigroup Triangular Mesh Discrete Ordinates Explicit Neutron Transport Code", LA-6735-M, Los Alamos National Laboratory (1977).

3. R. D. O'Dell, F. W. Brinkley, Jr., and D. Marr, "User's Manual for ONEDANT: A Code Package for One-Dimensional, Diffusion-Accelerated, Neutral-Particle Transport", LA-9184-M, Los Alamos National Laboratory (1982).

4. R. E. Alcouffe, et al, "User's Guide for TWODANT: A Code Package for Two-Dimensional, Diffusion-Accelerated, Neutral-Particle Transport", LA-10049-M, Los Alamos National Laboratory (1984).

5. E. W. Larsen, "Diffusion-Synthetic Acceleration Methods for Discrete-Ordinates Problems", *Transport Theory & Stat. Phys.*, **13**, 107 (1984).

6. H. J. Kopp, "Synthetic Method Solution of the Transport Equation", *Nucl. Sci. Eng.*, **17**, 65 (1963).

7. E. M. Gelbard and L. A. Hageman, "The Synthetic Method as Applied to the S_N Equations", *Nucl. Sci. Eng.*, **37**, 288 (1969).

8. W. H. Reed, "The Effectiveness of Acceleration Techniques for Iterative Methods in Transport Theory", *Nucl. Sci. Eng.*, **45**, 245 (1971).

9. R. E. Alcouffe, "A Stable Diffusion Synthetic Acceleration Mehtod for Neutron Transport Iterations", *Trans. Am. Nucl. Soc.*, **23**, 203 (1976).

10. R. E. Alcouffe, "Diffusion Synthetic Acceleration Methods for the Diamond-Differenced Discrete-Ordinates Equations", *Nucl. Sci. Eng.*, **64**, 344 (1977).

11. W. F. Miller, Jr., "Generalized Rebalance: A Common Framework for Transport Acceleration Methods", *Nucl. Sci. Eng.*, **65**, 226 (1978).

12. J. Aull, "The Stability of the Mesh-Cornered Synthetic Method of Diffusion Acceleration of the DOT-IV Transport Code", ORNL/TM-7097, Oak Ridge National Laboratory (1979).

13. J. Aull, "Acceleration of the Inner Iteration of the DOT-IV Transport Code Using a New Source Correction Scheme", ORNL/TM-7404, Oak Ridge National Laboratory (1980).

14. E. W. Larsen, "Unconditionally Stable Diffusion-Synthetic Acceleration Methods for the Slab Geometry Discrete Ordinates Equations. Part I: Theory", *Nucl. Sci. Eng.*, **82**, 47 (1982).

15. D. R. McCoy and E. W. Larsen, "Unconditionally Stable Diffusion-Synthetic Acceleration Methods for the Slab Geometry Discrete Ordinates Equations. Part II: Numerical Results", *Nucl. Sci. Eng.*, **82**, 64 (1982).

16. J. E. Morel, "A Synthetic Acceleration Method for Discrete Ordinates Calculations with Highly Anisotropic Scattering", *Nucl. Sci. Eng.*, **82**, 34 (1982).

17. H. Khalil, "A Nodal Diffusion Technique for Synthetic Acceleration of Nodal S_N Calculations", *Nucl. Sci. Eng.*, **90**, 263 (1985).

18. H. Khalil, "A Diffusion-Synthetic Acceleration Method for Acceleration of Linear Nodal S_N Calculations", *Trans. Am. Nucl. Soc.*, **53**, 278 (1986).

19. R. D. Lawrence, "An Interface-Current Approach to Synthetic Acceleration of Three-Dimensional Discrete-Ordinates Transport Methods", *Trans. Am. Nucl. Soc.*, **53**, 280 (1986).

20. M. L. Adams and W. R. Martin, "A New Approach to Synthetic Acceleration of Transport Calculations", *Trans. Am. Nucl. Soc.*, **53**, 282 (1986).

21. M. L. Adams, "A Synthetically-Accelerated Heterogeneous Response Matrix Method for Linear Transport Calculations", Ph.D thesis, The University of Michigan (1986).

22. R. E. Alcouffe, Los Alamos National Laboratory, Private Communication (1986).

23. E. W. Larsen and R. E. Alcouffe, "The Linear Characteristic Method for Spatially Discretizing the Discrete-Ordinates Equations in (X,Y)-Geometry", *Proc. International Conf. on Advances in Mathematical Methods for the Solution of Nuclear Engineering Problems*, p I-99 (1981).

24. H. Khalil, Argonne National Laboratory, Private Communication (1986).

25. E. W. Larsen, "Projected Discrete-Ordinates Methods for Numerical Transport Problems", *Nucl. Sci. Eng.*, **92**, 179 (1986).

26. P. Barbucci and F. Di Pasquantonio, "Exponential Supplementary Equations for S_N Methods: The One-Dimensional Case", *Nucl. Sci. Eng.*, **63**, 179 (1977).

27. R. E. Alcouffe, E. W. Larsen, W. F. Miller, Jr., and B. R. Wienke, "Computational Efficiency of Numerical Methods for the Multigroup, Discrete-Ordinates Neutron Transport Equations: The Slab Geometry Case", *Nucl. Sci. Eng.*, **71**, 111 (1979).

28. R. Vaidyanathan, "A Finite Moments Algorithm for Particle Transport Problems", *Nucl. Sci. Eng.*, **71**, 46 (1979).